

Probability density functions of power-in-bucket and power-in-fiber for an infrared laser beam propagating in the maritime environment

Charles Nelson,^{1,*} Svetlana Avramov-Zamurovic,² Olga Korotkova,³
Reza Malek-Madani,⁴ Raymond Sova,⁵ and Frederic Davidson⁶

¹Department of Electrical and Computer Engineering, United States Naval Academy, 105 Maryland Avenue, Annapolis, Maryland 21402, USA

²Department of Weapons and Systems Engineering, United States Naval Academy, 105 Maryland Avenue, Annapolis, Maryland 21402, USA

³Department of Physics, University of Miami, 1320 Campo Sano Drive, Coral Gables, Florida 33146, USA

⁴Department of Mathematics, United States Naval Academy, 105 Maryland Avenue, Annapolis, Maryland 21402, USA

⁵Johns Hopkins University Applied Physics Laboratory, 11100 Johns Hopkins Road, Laurel, Maryland 20723, USA

⁶Department of Electrical and Computer Engineering, Johns Hopkins University, 3400 N. Charles Street, Baltimore, Maryland 21218, USA

*Corresponding author: cnelson@usna.edu

Received 20 June 2013; revised 24 September 2013; accepted 19 September 2013;
posted 26 September 2013 (Doc. ID 192670); published 21 October 2013

Irradiance fluctuations of an infrared laser beam from a shore-to-ship data link ranging from 5.1 to 17.8 km are compared to lognormal (LN), gamma-gamma (GG) with aperture averaging, and gamma-Laguerre (GL) distributions. From our data analysis, the LN and GG probability density function (PDF) models were generally in good agreement in near-weak to moderate fluctuations. This was also true in moderate to strong fluctuations when the spatial coherence radius was smaller than the detector aperture size, with the exception of the 2.54 cm power-in-bucket (PIB) where the LN PDF model fit best. For moderate to strong fluctuations, the GG PDF model tended to outperform the LN PDF model when the spatial coherence radius was greater than the detector aperture size. Additionally, the GL PDF model had the best or next to best overall fit in all cases with the exception of the 2.54 cm PIB where the scintillation index was highest. The GL PDF model also appears to be robust for off-of-beam center laser beam applications. © 2013 Optical Society of America

OCIS codes: (010.1300) Atmospheric propagation; (010.1330) Atmospheric turbulence; (060.2605) Free-space optical communication; (030.7060) Turbulence; (290.5930) Scintillation.

<http://dx.doi.org/10.1364/AO.52.007449>

1. Introduction

The U.S. Navy relies heavily on radio frequency (RF) communication networks leading to two major operational limitations: low bandwidth and lack of

contingency capability in the event of jamming by adversaries [1,2]. One possible complementary solution to current RF systems is the use of free-space optical (FSO) communication links, which have inherently high-bandwidth and are highly directional, making them hard to detect or interfere with. FSO links have drawbacks as well: a laser beam propagating in a maritime environment can experience significant

random intensity fluctuations due to optical turbulence along the path and this in turn can lead to power loss at the receiver and degraded performance. Building a hybrid RF/optical system for the maritime environment can possibly provide the benefits of both systems.

Hybrid RF/optical communication systems have been considered and studied in a number of papers relating to airborne and military applications. In [1,3,4], the background, overview, and details of experiments and challenges with regard to the use of hybrid RF/optical communication applications are presented. In 2009, the Johns Hopkins University and Johns Hopkins University Applied Physics Laboratory initiated and executed an internal research and development effort to assess, demonstrate, and advance hybrid RF/optical communication links in the maritime environment. This research effort was successful and has been described at length in a number of references, see [2,5–7]. In this paper, we focus specifically on the probability density function (PDF) of the laser beam intensity in comparison with theoretical models.

The PDF of the fluctuating intensity is critical for estimation of the fade statistics of an optical signal and the bit-error rate of a communication system. Understanding PDF modeling as it relates to distance, scintillation level, detector type, and aperture size holds great benefit for optimizing the maritime communication link for a given turbulent channel. Many PDF models have been developed for laser beam propagation through the turbulent atmosphere including the lognormal (LN), gamma–gamma (GG), K, and LN modulated Rician or Beckmann, as well as others [8]. A thorough comparison of several PDF models for terrestrial links was made by McLaren *et al.* [9]. Perhaps the two most widely used PDF models are the LN and the GG. The LN PDF model has historically [10] been used for the weak fluctuation regime, and more recently, the GG PDF model has been proposed for the weak and strong fluctuation regimes [11]. In this paper we apply the LN and GG with modification to account for aperture averaging [12] PDF models as well as a PDF model proposed by Barakat [13], which we term the gamma-Laguerre (GL) PDF model.

Laser beam propagation in the maritime environment has been previously studied [14,15]. In [14], a research group with the Swedish Defence Research Agency performed a nearly six month study of 10.6 μm laser beam propagation over the Baltic Sea at ranges of 2.5, 5.5, and 16.5 km with single and double-pass links implemented with retroreflectors. Results of their study included refractive index structure parameter C_n^2 and scintillation index measurements, PDF model analysis (LN, gamma, and GG), as well as others. It was found that the LN PDF model had the overall best fit in most scenarios from weak to strong scintillation. In [15], the Naval Research Laboratory's Chesapeake Beach Detachment conducted a six month study of the scintillation index and the C_n^2 over a 16 km maritime link with a 1550 nm laser.

Their findings include detailed studies of the effects of the air and sea surface temperature differences on the value of C_n^2 as well as the scintillation index.

Experimental validation of several PDF models for laser beam intensity on the basis of a unique shore-to-ship continuous measurement is the main contribution of this paper. Specifically, we employ three different PDF models for an infrared (IR) laser beam captured as a near continuous function of propagation distance in the maritime environment from 5.1 km to near the optical horizon of 17.8 km. From our data analysis, the LN and GG PDF models were generally in good agreement in the near-weak to moderate fluctuation regime where the spatial coherence radius was larger than the detector aperture size and also in the moderate to strong fluctuation regime when the spatial coherence radius was smaller than the detector aperture size. This was true with the notable exception of the 2.54 cm power-in-bucket (PIB) where the LN PDF model demonstrated the best overall fit for cases where the spatial coherence radius was smaller than the detector aperture size. Also, for the moderate to strong fluctuation regime, the GG PDF model tended to outperform the LN PDF model when the spatial coherence radius was greater than the detector aperture size. These results are in general agreement with the findings from [16–18]. Additionally, we have observed that the GL PDF model had the best or next to best overall fit to the data for the near-weak, moderate, and strong fluctuation regime for all detectors with the exception of the 2.54 cm PIB where the scintillation index was highest. The GL PDF model also appears to be robust for off-of-beam center applications.

2. Theoretical Background

The PDF W of the normalized fluctuating beam intensity I , integrated between values a and b , gives the probability that the normalized intensity takes a value in the interval $[a, b]$, i.e.,

$$P(a \leq I \leq b) = \int_a^b W(I) dI. \quad (1)$$

In our work, we constructed the PDF from measured intensities by using the statistical moments computed directly from the data. We will now review three intensity PDF models for laser beam propagation: the GL [13], GG with aperture averaging [8,12] and the LN [19].

A. GL PDF Model

The approach introduced in [13] and discussed in [20], known as the GL PDF model utilizes the gamma distribution of light intensity I , normalized by its mean value, such that $\langle I \rangle = 1$, and is weighted by generalized Laguerre polynomials. It is given by the sum

$$W_{\text{GL}}(I) = W_g(I) \sum_{n=0}^{\infty} U_n L_n^{(\beta-1)} \left(\frac{\beta I}{\mu} \right), \quad I \geq 0, \quad (2)$$

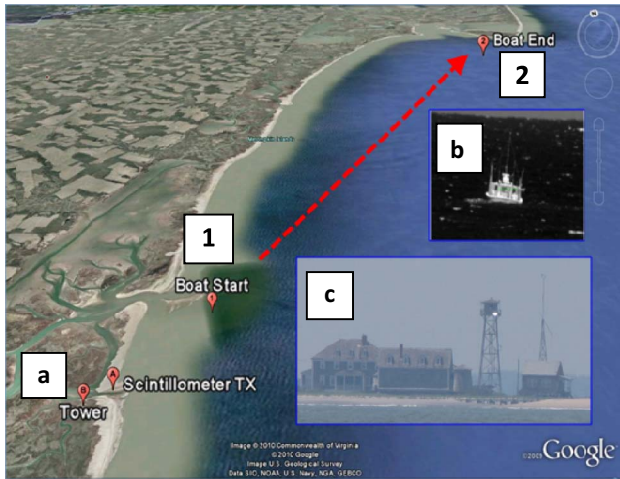
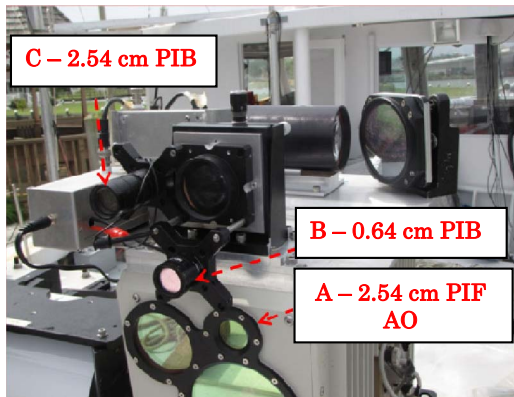
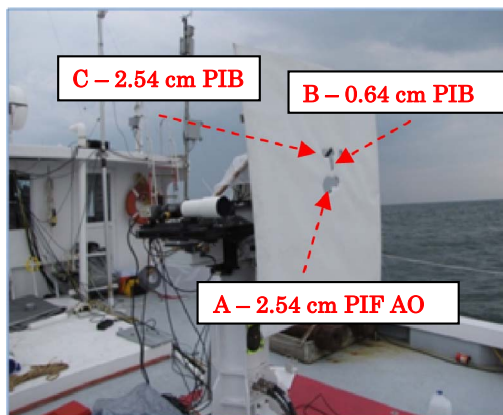


Fig. 1. Shore-to-ship, bi-directional 1550 nm optical link from the tower located at Cedar Island and research vessel traveling along the Atlantic Coast. (a) tower location, (b) picture of boat, and (c) picture of ~17 m tower, 1—boat starting point, 2—boat ending point [7,22].



(a)



(b)

Fig. 2. Experimental setup of instrumentation [7]. Devices relevant for the paper's analysis are highlighted. (a) 2.54 cm power-in-fiber adaptive optics (PIF AO) aperture, A; 0.64 and 2.54 cm PIB apertures, B and C, respectively; (b) 1.2 m x 1.2 m white screen for IR imaging of the overall optical beam. The cut-outs on the screen fit the detector apertures.

where $W_g(I)$ is the gamma distribution:

$$W_g(I) = \frac{1}{\Gamma(\beta)} \left(\frac{\beta}{\mu}\right)^\beta I^{\beta-1} \exp\left(-\frac{\beta I}{\mu}\right), \quad (3)$$

$\Gamma(x)$ being the gamma function and the two parameters, μ and β , of the distribution defined by the first and second moments:

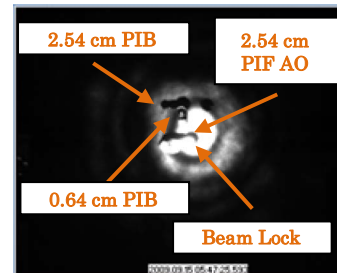
$$\mu = \langle I \rangle, \quad \beta = \langle I \rangle^2 / (\langle I^2 \rangle - \langle I \rangle^2). \quad (4)$$

The weighting coefficients, U_n , in Eq. (2) are found from the expression

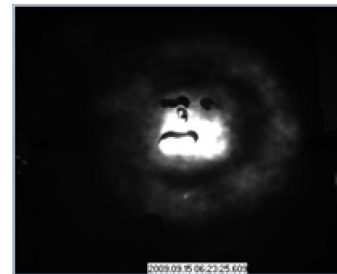
$$U_n = n! \Gamma(\beta) \sum_{k=0}^n \frac{(-\beta/\mu)^k \langle I^k \rangle}{k! (n-k)! \Gamma(\beta+k)}, \quad (5)$$

$U_0 = 1$, $U_1 = U_2 = 0$, while the generalized Laguerre polynomials $L_n^{(\beta-1)}(x)$ in Eq. (2) are given by

$$L_n^{(\beta-1)}(x) = \sum_{k=0}^n \binom{n+\beta-1}{n-1} \frac{(-x)^k}{k!}. \quad (6)$$



(a) 5.1 km



(b) 10.7 km



(c) 17.8 km

Fig. 3. IR spatial profiles of the propagating beam [7]. Location of detectors is as in (a).

It is recommended in [13] that the first five moments of the data should be used to ensure an accurate and stable approximation of the PDF. Additionally, as discussed in [21], caution must be observed when using higher-order measured moments so that they are not underestimated and that a sufficient number of data points must be observed to reduce scatter. The moments are given by

$$\langle I^n \rangle = \int_0^\infty I^n W(I) dI. \quad (7)$$

As done in [21], we looked at the fifth moment's integrand, given in Eq. (7) by $I^n W(I)$, where $n = 5$. For our case, we analyzed the data presented in Fig. 9(c) as a high-scintillation case and one well represented by the GL PDF model. From our analysis, the fifth moment's integrand increased to a maximum value of 17.8 at five times the normalized mean intensity value, and then decreased to a value of 1.1 at near the maximum data collection values of 10 times the normalized mean intensity value. From this, we judge the fifth measured moments not to be underestimated. Also, the probability for the GL PDF model at 10 times the normalized mean intensity was approximately 1 in 10,000, and with 600,000 data points analyzed for the comparison, we judge this to be a fair number of data points to reduce scatter in the higher-order moments. We note that for a clear presentation and comparison of the measured normalized intensity values, plots in this paper do not extend all the way out to the maximum values.

The significance of the GL PDF model is in its reliance only on the first several statistical moments of the data. The GL PDF model is included as an alternative to the GG PDF model for situations when no knowledge of atmospheric parameters or characteristics with regard to source, propagation distance, or atmospheric spectrum is required.

B. GG Aperture Averaged PDF Model

Perhaps the most widely used PDF model has become known as the GG PDF model [11]. For a finite detector size, as is the case for our experiment, the GG PDF model is modified to include aperture averaging (GG_A) [12]. The GG_A PDF model is given by the formula

$$W_{GG_A}(I) = \frac{2(\alpha\beta_G)^{\frac{\alpha+\beta_G}{2}}}{\Gamma(\alpha)\Gamma(\beta_G)} I^{\frac{\alpha+\beta_G}{2}-1} K_{\alpha-\beta_G}(2\sqrt{\alpha\beta_G I}), \quad I > 0, \quad (8)$$

where $\Gamma(x)$ is the gamma function, as before, $K_m(x)$ is the modified Bessel function of the second kind, I is

the normalized intensity, and the parameters α and β_G are defined as follows:

$$\alpha = \frac{1}{\exp(\sigma_{\ln x}^2) - 1}, \quad \beta_G = \frac{1}{\exp(\sigma_{\ln y}^2) - 1}. \quad (9)$$

Here $\sigma_{\ln x}^2$ and $\sigma_{\ln y}^2$ are the large and small scale log-irradiance variances. With aperture averaging, and for the Kolmogorov power spectrum, these quantities are given in [12]:

$$\sigma_{\ln x}^2 \cong 0.49\sigma_1^2 \left(\frac{\Omega_G - \Lambda_1}{\Omega_G + \Lambda_1} \right)^2 \left(\frac{1}{3} - \frac{1}{2}\bar{\Theta}_1 + \frac{1}{5}\bar{\Theta}_1^2 \right) \times \left[\frac{\eta_x}{1 + 0.40\eta_x \frac{(2-\bar{\Theta}_1)}{(\Lambda_1 + \Omega_G)}} \right]^{\frac{7}{6}}, \quad (10)$$

$$\sigma_{\ln y}^2 \cong \frac{1.27\sigma_1^2\eta_y^{-5/6}}{1 + \frac{0.40\eta_y}{(\Lambda_1 + \Omega_G)}}, \quad \eta_y \gg 1, \quad (11)$$

where,

$$\eta_x = \frac{\left(\frac{1}{3} - \frac{1}{2}\bar{\Theta}_1 + \frac{1}{5}\bar{\Theta}_1^2 \right)^{-\frac{6}{7}} \left(\frac{\sigma_B}{\sigma_1} \right)^{\frac{12}{7}}}{1 + 0.56\sigma_B^{\frac{12}{5}}}, \quad (12)$$

$$\eta_y = 3 \left(\frac{\sigma_1}{\sigma_B} \right)^{12/5} \left(1 + 0.69\sigma_B^{12/5} \right), \quad (13)$$

$$\Lambda_1 = \frac{\left(\frac{2L}{kW_0^2} \right)}{1 + \left(\frac{2L}{kW_0^2} \right)^2}, \quad (14)$$

$$\Omega_G = \frac{16L}{kD^2}, \quad (15)$$

where D is the aperture diameter of the detector,

$$\bar{\Theta}_1 = 1 - \Theta, \quad (16)$$

$$\Theta = \left[1 + \left(\frac{2L}{kW_0^2} \right)^2 \right]^{-1}, \quad (17)$$

$$\sigma_B^2 = (\langle I^2 \rangle - \langle I \rangle^2) / \langle I \rangle^2, \quad (18)$$

$$\sigma_1^2 \cong \frac{\sigma_{\text{RGB}}^2}{3.86 \left\{ 0.40 \left[(1 + 2\Theta)^2 + 4\Lambda_1^2 \right]^{\frac{5}{2}} \cos \left[\frac{5}{6} \tan^{-1} \left(\frac{1+2\Theta}{2\Lambda_1} \right) \right] - \frac{11}{16} \Lambda_1^{5/6} \right\}}, \quad (19)$$

$$\sigma_{\text{RGB}}^2 \cong \sigma_B^2. \quad (20)$$

In these expressions Θ and Λ_1 are the refraction and diffraction parameters in the receiver plane, respectively, for a collimated beam, W_0 is the initial beam radius, L is the propagation distance from the source to receiver, $k = 2\pi/\lambda$ is the wave number, σ_B^2 , is the scintillation index computed directly from the data, and σ_1^2 is the plane wave Rytov variance. As noted in Eq. (20), σ_{RGB}^2 (the symbol σ_B^2 is used in [12], since we use σ_B^2 for scintillation index, σ_{RGB}^2 is used) is approximated by the scintillation index, σ_B^2 , as measured from the data and given by Eq. (18). This is justified for the weak fluctuation regime where the on-axis variance of the log-irradiance given by $\sigma_{\ln I}^2 = \sigma_{\text{RGB}}^2$, is approximately equal to the

scintillation index, or $\sigma_{\ln I}^2 \cong \sigma_B^2$ [12]. For our experiment, the data suggests that the optical scintillation extends from the near-weak fluctuation regime (shorter-range data set) and into the moderate to strong fluctuation regime (mid to longer range data sets). We did not observe a significant difference in performance of the GG_A PDF model as compared to the GG PDF without aperture-averaging where the assumption of Eq. (20) is not made. Additionally, the detectors were physically located near beam center (see Section 3), and with the exception of the near range data (5.1 km), we did not observe a noticeable effect on the PDF models when detectors were located just off-of the beam center for the other ranges, and we judge Eq. (20) to be reasonable.

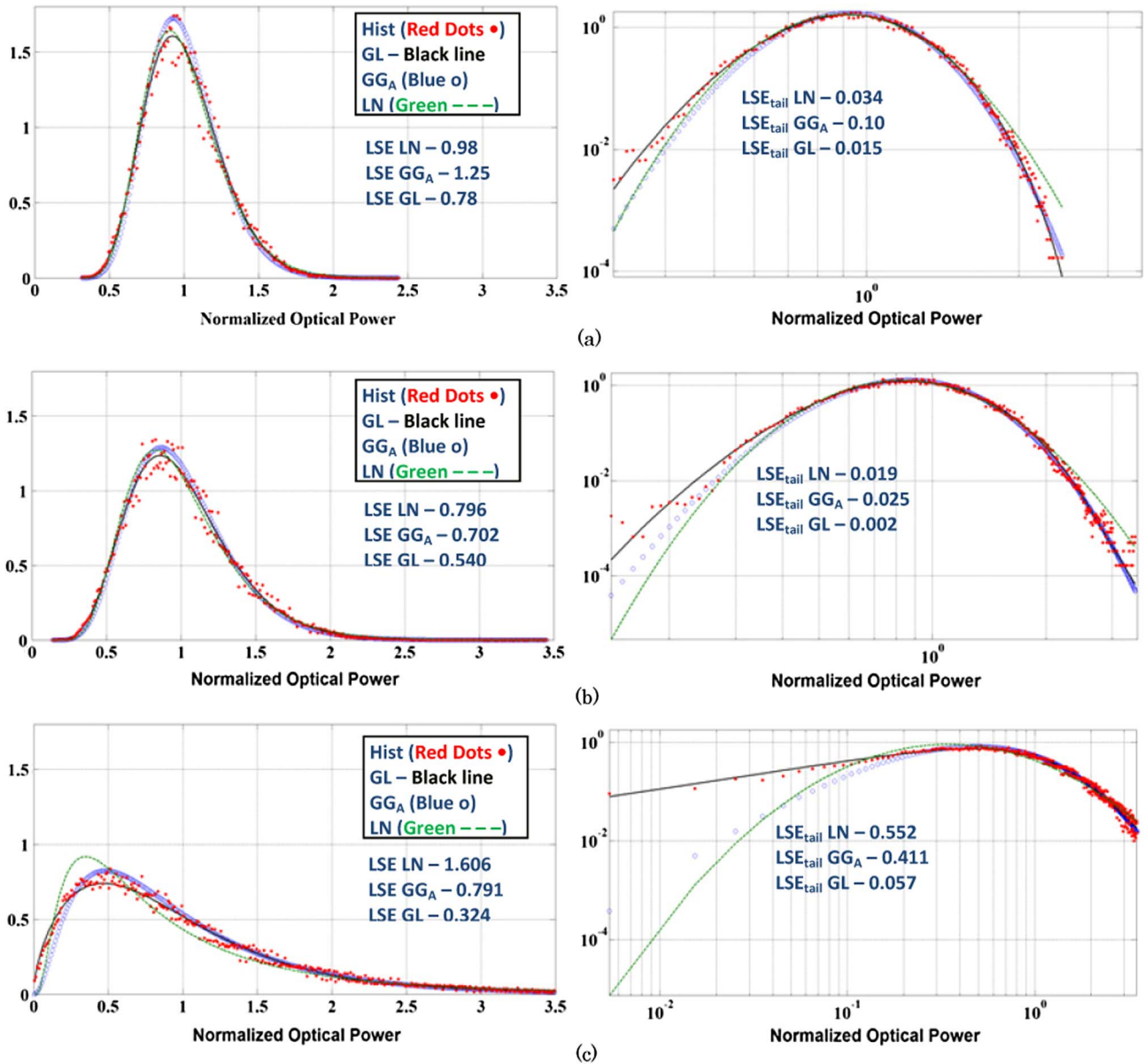


Fig. 4. PDF models and histogram for Case I using a 2.54 cm PIF communication terminal with an IR laser at $\lambda = 1550$ nm. (a) 5.1 km, computed scintillation index, $\sigma_B^2 = 0.066$, $\rho_0 \sim 4.1$ cm, $\sigma_R^2 \sim 1.0$. (b) 10.7 km, computed scintillation index, $\sigma_B^2 = 0.123$, $\rho_0 \sim 3.2$ cm, $\sigma_R^2 \sim 3.7$. (c) 17.8 km, computed scintillation index, $\sigma_B^2 = 0.63$, $\rho_0 \sim 2.6$ cm, $\sigma_R^2 \sim 9.4$.

C. LN PDF Model

We use the LN PDF model in our analysis because it is a classic and proven weak fluctuation regime PDF model. The LN PDF model is a two-parameter model given by [19]:

$$W_{\text{LN}}(I) = \frac{1}{I\sigma_{\ln I}\sqrt{2\pi}} \exp\left[-\frac{[\ln(I) - \mu_{\ln I}]^2}{2\sigma_{\ln I}^2}\right], \quad I > 0, \quad (21)$$

where I is the normalized intensity, $\mu_{\ln I}$ is the mean, and $\sigma_{\ln I}^2$ is the variance of the log-irradiance, respectively: $\mu_{\ln I} = \langle \ln(I) \rangle$, $\sigma_{\ln I}^2 = \text{var}(\ln(I))$.

3. Experiment Description

Figure 1 illustrates the shore-to-ship, bi-directional optical link near Wallops Island, VA on the Atlantic Coast. The research vessel [Fig. 1(b)], started at point 1, approximately 5.1 km from the ~17 m tower [Fig. 1(c)] and proceeded at approximately 2 m/s out to almost the horizon distance of 17.8 km at point 2. Pointing and tracking lock was maintained and data collected near continuously over this propagation path. Figure 2 illustrates the experimental setup, showing the location of the detectors on the research vessel as well as the screen used for filming the spatial profile of the propagating laser beam.

Additional fine detail of the experimental setup as well as environmental and channel characterization

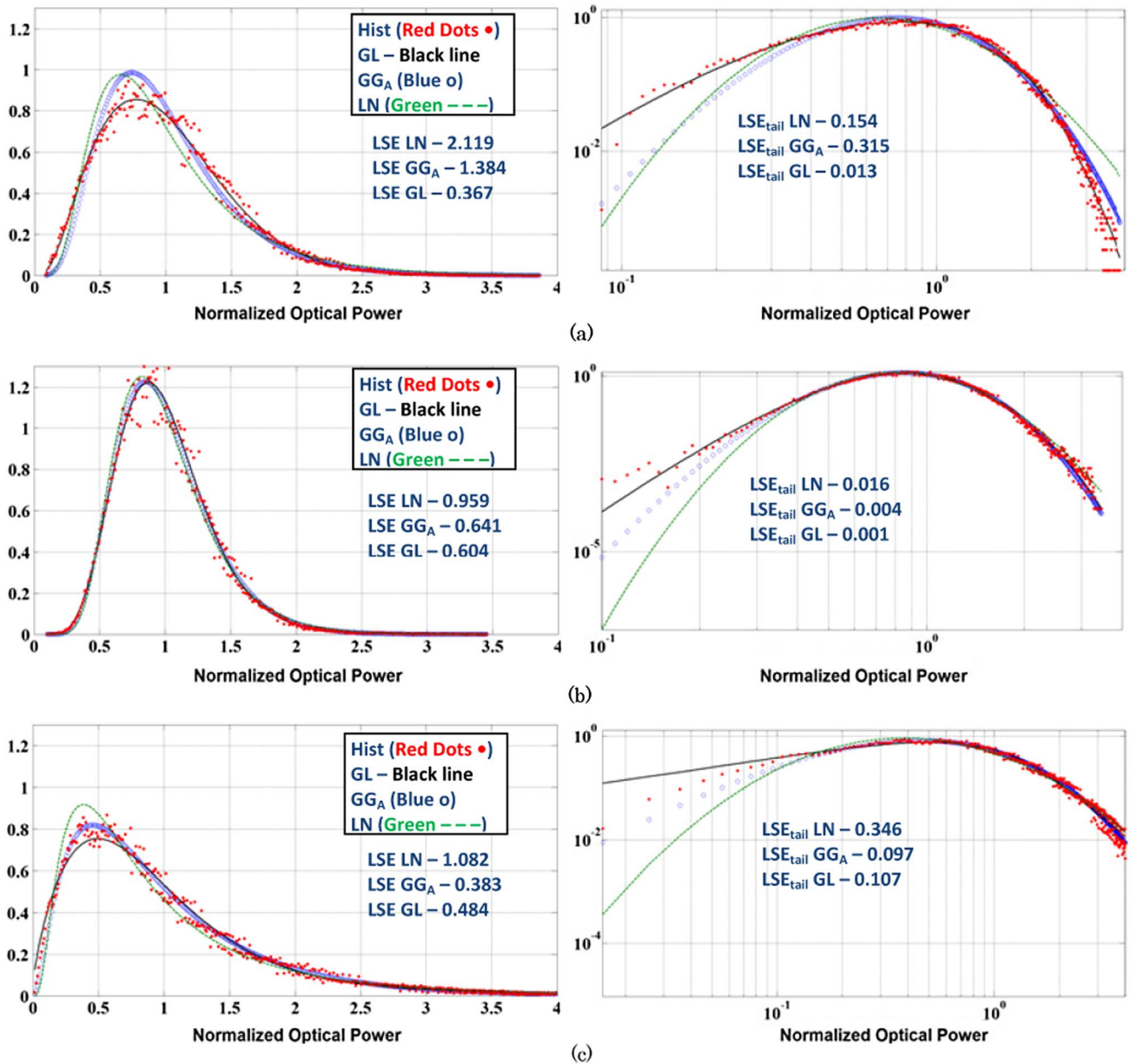


Fig. 5. PDF models and histogram for Case I using a 0.64 cm PIB aperture detector with an IR laser at $\lambda = 1550$ nm (a) 5.1 km, computed scintillation index, $\sigma_B^2 = 0.238$, $\rho_0 \sim 4.1$ cm, $\sigma_R^2 \sim 1.0$. (b) 10.7 km, computed scintillation index, $\sigma_B^2 = 0.129$, $\rho_0 \sim 3.2$ cm, $\sigma_R^2 \sim 3.7$. (c) 17.8 km, computed scintillation index, $\sigma_B^2 = 0.632$, $\rho_0 \sim 2.6$ cm, $\sigma_R^2 \sim 9.4$.

and analysis are presented in [2]; highlights are repeated here for clarity. Specifically, during tests, the IR (1550 nm) laser beam center was locked between the 2.54 cm power-in-fiber adaptive optics (PIF AO Fig. 2, labeled A) aperture of the boat and the 10 cm PIF aperture of the tower (not shown). Additionally, two PIB detectors of 0.64 cm (PIB Fig. 2 labeled B) and 2.54 cm (PIB Fig. 2 labeled C) diameter were located close to the 2.54 cm PIF AO detector. Further, a 1.2 m × 1.2 m screen [Fig. 2(b)] was used to capture the spatial profile of the propagating IR laser beam. From the environmental characterizations, the turbulence conditions were estimated to be relatively stable over each data run (see Section 4) and in line with analysis from [2]. This atmospheric

stability for each run allows for reasonable comparisons of the data as a function of range.

4. Methodology

This paper presents analysis of IR laser beam propagation under generally moderate optical turbulence conditions in the maritime environment with path averaged values of the refractive index structure parameter, C_n^2 , estimated to be $\sim 2.4 \cdot 10^{-15} \text{ m}^{-2/3}$ for Case I and $\sim 5.2 \cdot 10^{-15} \text{ m}^{-2/3}$ Case II. Since the beam was actively tracked using AO, we may assume that the beam radius is determined by its short-term beam radius, W_{ST} , as computed from [8]. IR spatial images were taken at 60 frames/s and between four and 10 consecutive images were averaged to produce

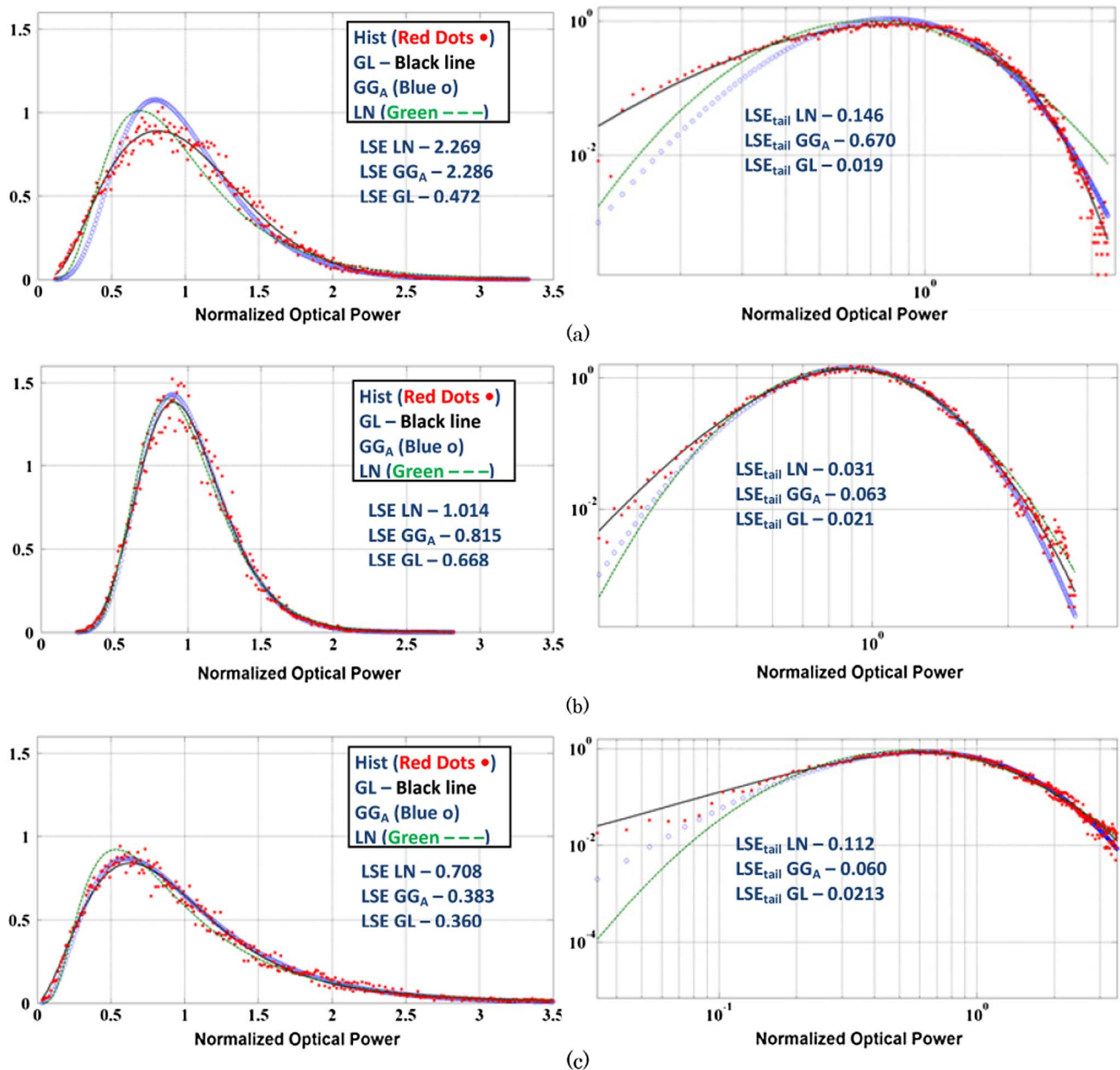


Fig. 6. PDF models and histogram for Case I using a 2.54 cm PIB aperture detector with an IR laser at $\lambda = 1550 \text{ nm}$. (a) 5.1 km, computed scintillation index, $\sigma_B^2 = 0.209$, $\rho_0 \sim 4.1 \text{ cm}$, $\sigma_R^2 \sim 1.0$. (b) 10.7 km, computed scintillation index, $\sigma_B^2 = 0.097$, $\rho_0 \sim 3.2 \text{ cm}$, $\sigma_R^2 \sim 3.7$. (c) 17.8 km, computed scintillation index, $\sigma_B^2 = 0.417$, $\rho_0 \sim 2.6 \text{ cm}$, $\sigma_R^2 \sim 9.4$.

a composite spatial image for each of the three distances presented. W_{ST} was estimated by first measuring the number of pixels from both the vertical and horizontal cross sections of the beam as measured from approximately the first diffraction ring null. The number of pixels was converted to meters using the known size of the screen in pixels and then the two diameters were divided by 2 to get the radius. As W_{ST} is a function of C_n^2 , the C_n^2 that gave the best fit to W_{ST} was determined and then averaged over the three distances presented. This estimation procedure is similar to the one utilized in [2]. Additionally, as performed in [2], we analyzed the air temperature located at 5 m above the water and sea water intake temperature (SWIT) located just below the surface for each data run. The $T_{AIR} - T_{SWIT}$ difference varied approximately between negative 1 and negative 2 degrees Celsius for Case I and between zero and positive 1.5 degrees Celsius for Case II. For similar air and sea temperature differences in [15] the resulting estimated change in C_n^2 was on the order of $\sim 2 \cdot 10^{-15} \text{ m}^{-2/3}$ in the Chesapeake Bay. We judge this variability in C_n^2 to be reasonably stable over the time of our data runs. Similar conclusions were made in [2].

The data plots (see Section 5) include scintillation index, σ_B^2 given by Eq. (18) and computed directly from the measured data, propagation distance, approximate Rytov variance σ_R^2 and estimated spatial coherence radius ρ_0 . Additionally, ship and wind speed and direction as measured on the boat are included at the beginning of each case section. The Rytov variance σ_R^2 and estimated spatial coherence radius ρ_0 , for a Gaussian beam, are computed from the expressions [8]:

$$\sigma_R^2 = 1.23 C_n^2 k^7 L^{11/6}, \quad (22)$$

$$\rho_0 = \left[\frac{8}{3(a + 0.62\Lambda_1)^{1/6}} \right]^{3/8} (1.46 C_n^2 k^2 L)^{-3/8},$$

$$l_0 \ll \rho_0 \ll L_0, \quad (23)$$

where

$$a = \frac{1 - \Theta^{3/8}}{1 - \Theta}, \quad \Theta \geq 0,$$

and l_0 and L_0 are the inner and outer scales of turbulence, respectively. For the cases presented, ρ_0 is estimated to fall in the range of 2–5 cm, l_0 near ground level is typically between 1 and 10 mm, and L_0 is usually assumed to grow linearly with the order of the height above ground [8]; from this we assume $l_0 \ll \rho_0 \ll L_0$ is valid. In general, $\sigma_R^2 < 1$ defines the weak fluctuation regime and $\sigma_R^2 > 1$ the moderate to strong fluctuation regime. For the data presented in Case I, near weak to moderate is defined as $\sigma_R^2 \sim 1$ to 3.7 and moderate to strong for $\sigma_R^2 > 3.7$. For Case II, σ_R^2 is greater than ~ 3.6 for

all data points and is considered to be in the moderate to strong fluctuation regime for all data.

As discussed, PDF models in this paper represent normalized fluctuating power levels at the detectors on or near the beam center. This condition was achieved through a locked link. Additionally, the LN, GG_A, and GL PDF models are computed directly from moments of the data. Curve fitting routines to estimate the parameters of the PDF models are often used in the literature, but to achieve a fair comparison with the GL PDF model, which is built up directly from moments of the data, we did not use curve fitting in this paper. The histograms and PDF models are presented as functions of one, two, or three different propagation distances as well as functions of three different apertures: 0.64 and 2.54 cm PIB, and 2.54 cm PIF AO. Observed realizations are one minute long to achieve a reasonable number of observations of intensity fluctuations. The research vessel's average speed through the water was about 2 m/s, giving reasonably constant conditions over the observation time.

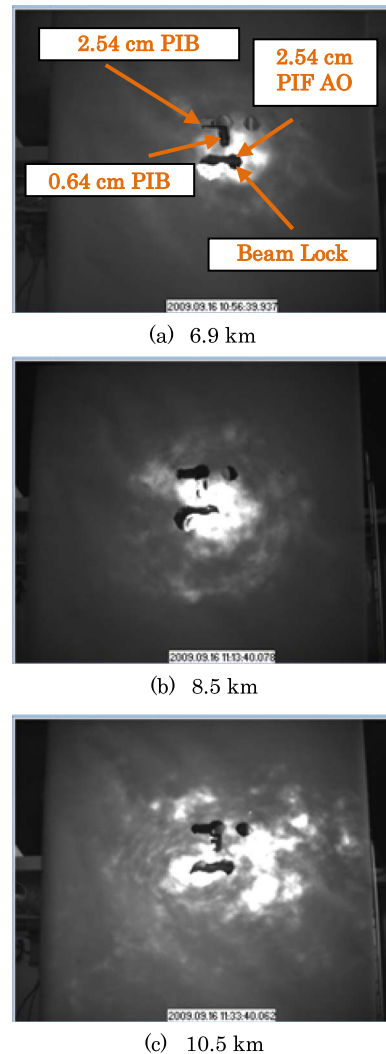


Fig. 7. IR spatial profiles of the propagating beam [7]. Location of detectors is as in (a).

The samples of data were collected at 10,000 samples/s or 600,000 data points for the 1 min observation time and then normalized to the mean of the data. Normalized data is used to calculate moments for the PDF models and to build histograms with 100 bins per mean value of optical power. The histograms were compared to the PDF models and the performance measure used was least squared error (LSE).

The LSE value was computed as follows. The value at the histogram bin center was used to calculate the probability of the PDF model at that intensity value, and then the difference between the histogram data value and the PDF model value at that histogram bin center was squared and summed across the number

of bins to give the total LSE value. Additionally, the LSE for the first 30 bins was computed to give a comparison between different models on the left end of the PDF. The left tail is an important aspect for communication applications because it substantially affects the fade-statistics of the channel.

5. Results

A. Moderate Turbulence Case I—Path Averaged $C_n^2 \sim 2.4 \cdot 10^{-15} \text{ M}^{-2/3}$ (Early Morning)— $\sigma_R^2 \sim 1.0$ To 9.4—5.1 km, 10.7 km, and 17.8 km Propagation Distances

The images in Fig. 3 show the spatial profile of the IR laser beam as captured at 5.1, 10.7, and near the horizon distance of 17.8 km. The spatial profile of

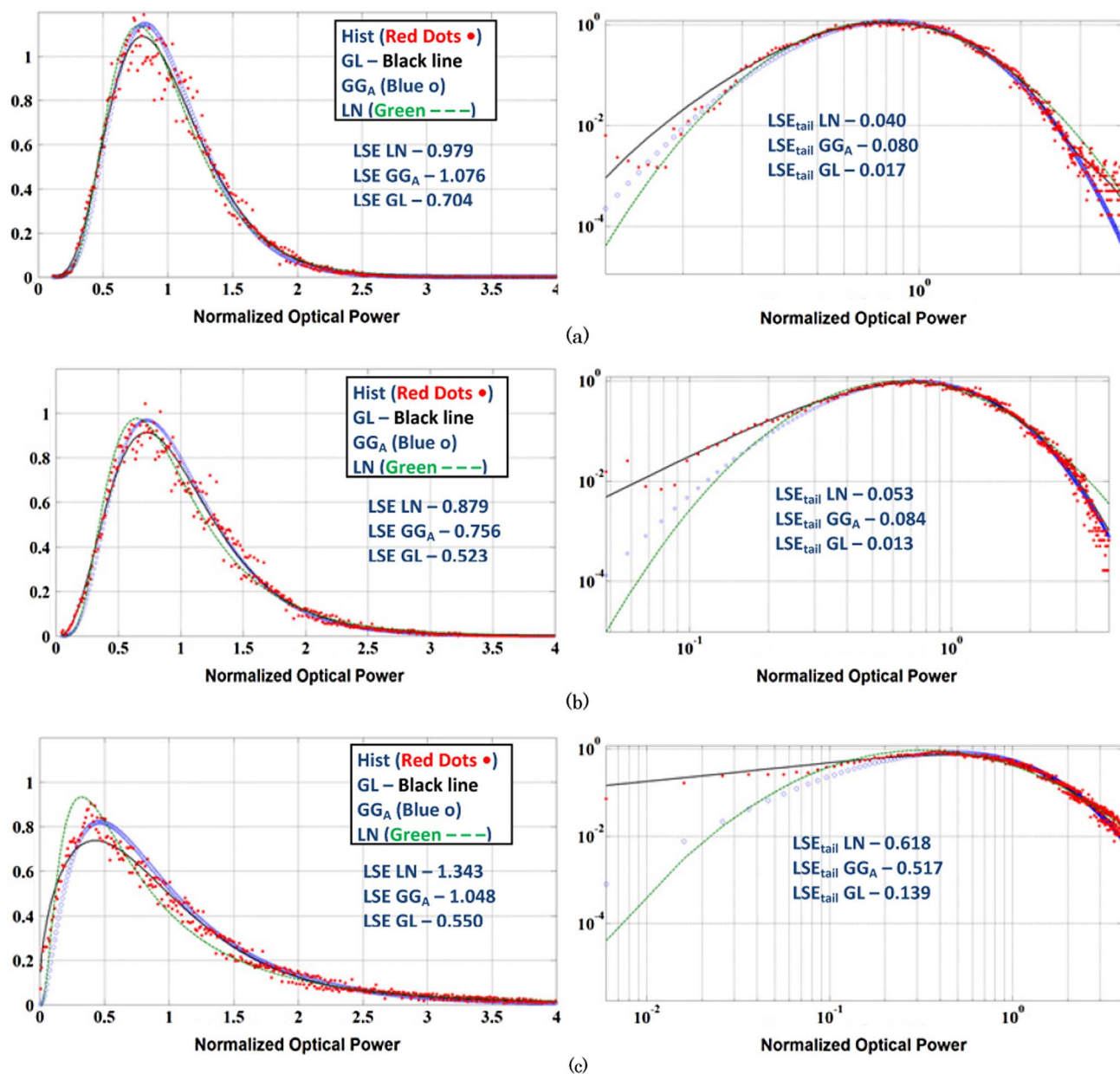


Fig. 8. PDF models and histogram for Case II using a 2.54 cm PIF communication terminal with an IR laser at $\lambda = 1550 \text{ nm}$. (a) 6.9 km, computed scintillation index, $\sigma_B^2 = 0.172$, $\rho_0 \sim 2.4 \text{ cm}$, $\sigma_R^2 \sim 3.6$. (b) 8.5 km, computed scintillation index, $\sigma_B^2 = 0.279$, $\rho_0 \sim 2.2 \text{ cm}$, $\sigma_R^2 \sim 5.2$. (c) 10.5 km, computed scintillation index, $\sigma_B^2 = 0.706$, $\rho_0 \sim 2.1 \text{ cm}$, $\sigma_R^2 \sim 7.7$.

the beam is provided to give qualitative information and insight on the status of the propagating beam, including relative size and speckle structure, which can be related to atmospheric and turbulence conditions. For the following set of data, the ship was at speed of ~ 2 m/s and on course of approximately 060 true with an average wind speed fluctuating between ~ 2 –5 m/s from $\sim 200^\circ$ true, giving a cross beam wind profile $\sim 40^\circ$ to the propagation path.

Figures 4–6 show the histograms and PDF models for the 2.54 cm PIF detector, the 0.64 cm PIB detector, as well as the 2.54 cm PIB detector, respectively. Plots on the left-hand side are on a linear x axis and y axis to show the overall shape and plots on the right are log x axis and log y axis are to give a picture of the data in the left tail.

For the cases of the PIB detectors [0.64 and 2.54 cm, Figs. 5(a) and 6(a)], the PDF models display noticeable differences at the 5.1 km distance. We suggest that at this short range, the PIB detector's—located just off-center of beam lock—may only be capturing the fringes of the beam [see Fig. 3(a)], and this accounts for the observed difference. Also, this fringing effect can be observed in the reduction of the scintillation index of the two PIB detectors when going from short range [5.1 km, see Figs. 5(a) and 6(a)] to medium range [10.7 km, see Figs. 5(b) and 6(b)]. Notably, the GL PDF model shows an excellent fit to the data collected off of beam center at 5.1 km, and especially in the left tail. For longer ranges, in the moderate to strong fluctuation regime, and where the estimated spatial coherence radius,

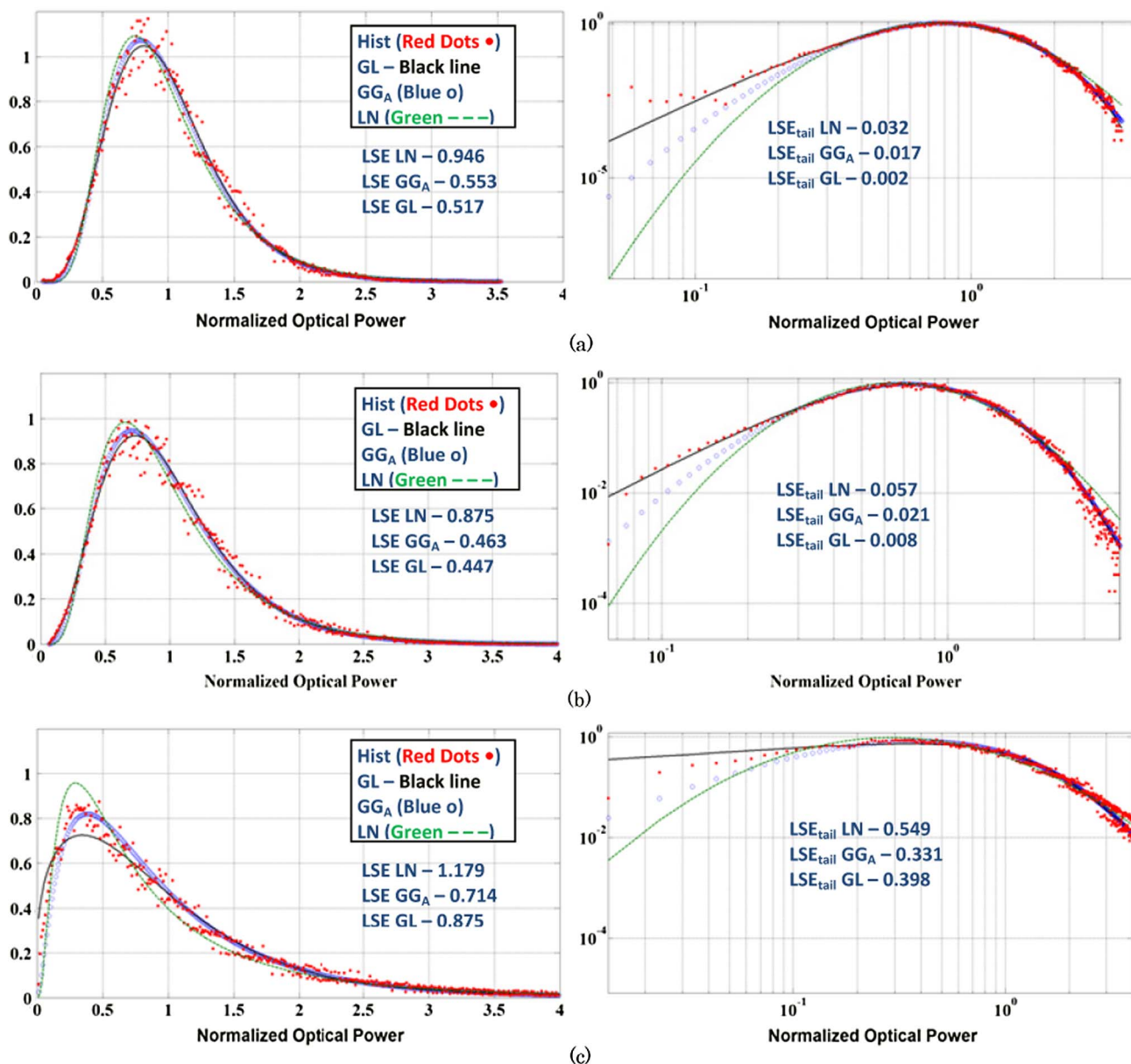


Fig. 9. PDF models and histogram for Case II using 0.64 cm PIB aperture detector with an IR laser at $\lambda = 1550$ nm. (a) 6.9 km, computed scintillation index, $\sigma_B^2 = 0.184$, $\rho_0 \sim 2.4$ cm, $\sigma_R^2 \sim 3.6$. (b) 8.5 km, computed scintillation index, $\sigma_B^2 = 0.273$, $\rho_0 \sim 2.2$ cm, $\sigma_R^2 \sim 5.2$. (c) 10.5 km, computed scintillation index, $\sigma_B^2 = 0.790$, $\rho_0 \sim 2.1$ cm, $\sigma_R^2 \sim 7.7$.

ρ_0 , was greater than the detector aperture size, the GG_A and GL PDF models showed generally improved fits as compared with the LN PDF model.

For the case of the PIF detector (2.54 cm, Fig. 4), all of the PDF models demonstrated generally comparable fits at 5.1 and 10.7 km distance, but diverged at the 17.8 km distance. At 17.8 km distance, where the overall scintillation was in the reasonably strong fluctuation regime, and where the estimated spatial coherence radius ρ_0 was greater than the detector size, the GG_A demonstrated a better overall fit than the LN PDF model.

While all of the PDF models appear to fit the data reasonably well across the different ranges and fluctuation regimes for Case I, the GG_A and GL PDF

models generally fit the data better overall as compared with the LN PDF model. Additionally, as noted, where the optical scintillation was in the moderate to strong fluctuation regime, and the estimated spatial coherence radius ρ_0 was greater than the aperture diameters of the detectors, the PDFs tended to be more GG_A than LN. This is in general agreement with what was observed in [16–18].

B. Moderate Turbulence Case II—Path Averaged $C_n^2 \sim 5.2 \cdot 10^{-15} M^{-2/3}$ (Mid-Day)— $\sigma_R^2 \sim 3.6$ to 7.7–6.9, 8.5, and 10.5 km Propagation Distances

The images in Fig. 7 show the spatial profile of the IR laser beam as captured at 6.9 and 10.5 km. For the following set of data, the ship speed was ~ 2 m/s and

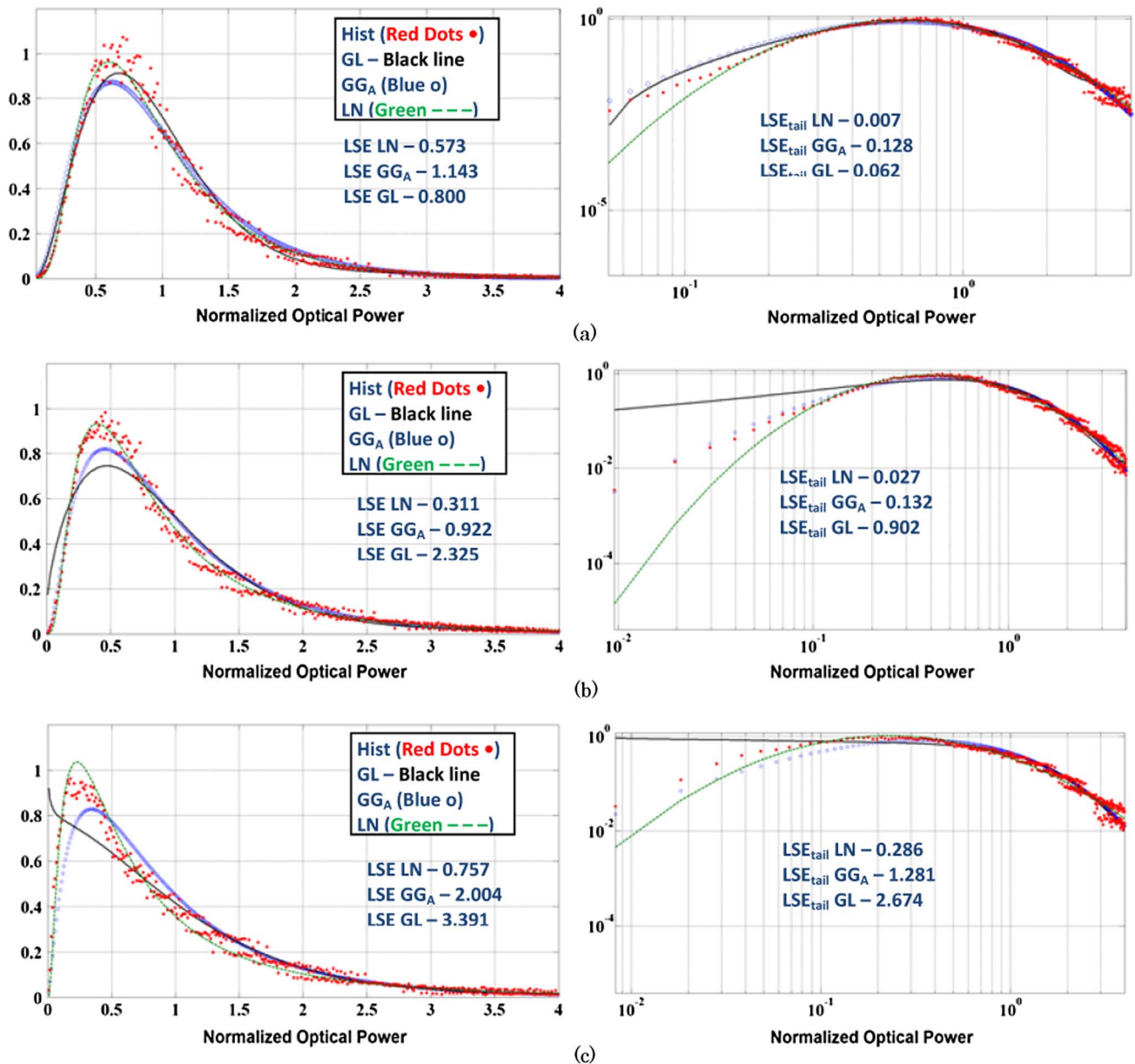


Fig. 10. PDF models and histogram for Case II using 2.54 cm PIB aperture detector with an IR laser at $\lambda = 1550$ nm. (a) 6.9 km, computed scintillation index, $\sigma_B^2 = 0.436$, $\rho_0 \sim 2.4$ cm, $\sigma_R^2 \sim 3.6$. (b) 8.5 km, computed scintillation index, $\sigma_B^2 = 0.750$, $\rho_0 \sim 2.2$ cm, $\sigma_R^2 \sim 5.2$. (c) 10.5 km, computed scintillation index, $\sigma_B^2 = 1.08$, $\rho_0 \sim 2.1$ cm, $\sigma_R^2 \sim 7.7$.

on course of approximately 060 true with an average wind speed fluctuating between $\sim 4\text{--}7$ m/s from $\sim 50^\circ$ true, giving a cross beam wind profile $\sim 10^\circ$ to the propagation path. The detector locations are the same as in Fig. 3(a) and repeated in Fig. 7(a).

Figures 8–10 show the histograms and PDF models for the 2.54 cm PIF detector, the 0.64 cm PIB detector, as well as the 2.54 cm PIB detector. As before, plots on the left-hand side are on a linear x axis and y axis to show the overall shape and plots on the right are log x axis and log y axis to give a picture of the data in the left tail.

For Case II, the optical turbulence was greater than for Case I, and is evident in the size of the scintillation index for comparable distances between Case I and Case II. For the PIF (Fig. 8), the LN and GG_A PDF models have reasonably comparable fits over all ranges, with the GL PDF model having the overall best fit.

For the PIB detectors, as with Case I, in the case of the 0.64 cm PIB detector (Fig. 9) the GG_A and GL PDF models show a better overall fit as compared with the LN PDF model. For the 2.54 cm PIB detector (Fig. 9), the LN PDF model has the best overall fit for all ranges. This may be explained as follows, from the theory on aperture averaging, the fastest fluctuations caused by small scale sizes average out, which leads to the measured scintillation being produced by scale sizes larger than the aperture. Therefore, in stronger turbulence, if the small-scale scintillation is mostly averaged out, this would shift the PDF toward the distribution of the large-scale fluctuations, or the LN PDF model [17]. This shift to the LN PDF model is observed in our data and is in alignment with findings from [16–18]. Of note, if the LN PDF model has the best fit for the 2.54 cm PIB detector, and the spatial coherence radius ρ_0 was smaller than the size of the detector, then why were similar results not seen for the 2.54 cm PIF detector? The possible explanation for this is explored in the discussion preceding Fig. 11 where we suggest the effective diameter of the PIF detector could be less than 2.54 cm.

Of additional note, is that with the higher scintillation observed for the 2.54 cm PIB detector [Figs. 10(b) and 10(c)], the GL PDF model starts to shift toward a negative exponential and no longer performs as well compared with previous data sets.

A point of interest is that, as can be seen in Fig. 11, the 2.54 cm PIF AO detector and the 0.64 cm PIB detector distributions appear nearly identical for Case I and Case II turbulence conditions (only Case I is shown, Fig. 11). The additional aperture averaging of the 2.54 cm PIF AO detector as compared with the 0.64 cm PIB detector, would lead us to expect different PDF distributions across the ranges. This is not generally observed in our data. One possibility for this similarity is the effect of the single-mode fiber serving as a spatial frequency filter for the focused light collected in the 2.54 cm PIF AO detector. In effect, this causes it to “look” similar to the 0.64 cm PIB detector. Spatial filtering is discussed in a

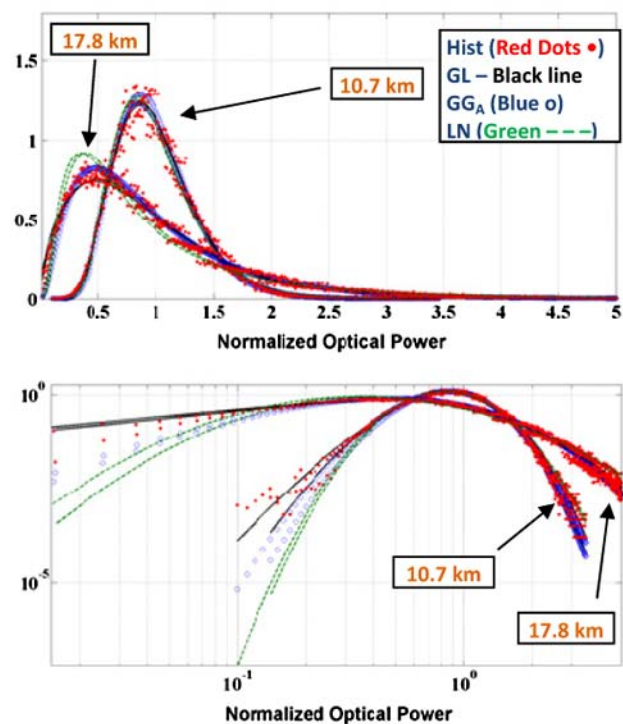


Fig. 11. Comparison of PDF models and histogram [Figs. 4(b), 4(c) and 5(b), and 5(c) are overlapped] for Case I at 10.7 and 17.8 km using a 2.54 cm PIF and 0.64 cm PIB aperture detectors.

number of papers on stellar interferometry [23] as an example.

6. Conclusions

In summary, a 2.54 cm PIF, and two PIB (0.64 and 2.54 cm) detectors were used to collect data for an IR laser beam propagating in the maritime environment over varying distance and levels of optical turbulence. Three PDF models, the GL, GG_A , and the LN PDF models were analyzed. From our data analysis, the LN and GG PDF models were generally in good agreement in the near weak to moderate fluctuation regime where the spatial coherence radius was larger than the detector aperture size and also in the moderate to strong fluctuation regime when the spatial coherence radius was smaller than the detector aperture size. This was true with the notable exception of the 2.54 cm PIB where the LN PDF model demonstrated the best overall fit for cases where the spatial coherence radius was smaller than the detector aperture size. Also, for the moderate to strong fluctuation regime, the GG PDF model tended to outperform the LN PDF model when the spatial coherence radius was greater than the detector aperture size. Additionally, we have observed that the GL PDF model had the best or next to best overall fit to the data for the near-weak, moderate, and strong fluctuation regime for all detectors with the exception of the 2.54 cm PIB where the scintillation index was highest. The GL PDF model also appears to be robust for off-of-beam center applications.

Our team would like to acknowledge the support from ONR N0001412WX20146 for Dr. Avramov-Zamurovic, and AFOSR FA9550-12-1-0449 for Dr. Korotkova's research, and the support from the Johns Hopkins University Applied Physics Laboratory. Additionally, we would like to acknowledge and thank our reviewers for several helpful comments.

References

1. S. Das, H. Henniger, B. Epple, C. I. Moore, W. Rabinovich, R. Sova, and D. Young, *Requirements and Challenges for Tactical Free-Space Lasercomm* (Milcom, 2008).
2. J. C. Juarez, J. E. Sluz, C. Nelson, M. B. Airola, M. J. Fitch, D. W. Young, D. Terry, F. M. Davidson, J. R. Rottier, and R. M. Sova, "Free-space optical channel characterization in the maritime environment," *Proc. SPIE* **7685**, 76850H (2010).
3. J. C. Juarez, A. Dwivedi, A. R. Hammons, Jr., S. D. Jones, V. Weerackody, and R. A. Nichols, "Free-space optical communications for next-generation military networks," *IEEE Commun. Mag.* **44**(11), 46–51 (2006).
4. L. B. Stotts, L. C. Andrews, P. C. Cherry, J. J. Foshee, P. J. Kolodzy, W. K. McIntire, M. Northcott, R. L. Phillips, H. A. Pike, B. Stadler, and D. W. Young, "Hybrid optical RF airborne communications," *Proc. IEEE* **97**, 1109–1127 (2009).
5. J. Juarez, J. Sluz, C. Nelson, F. Davidson, D. Young, and R. Sova, "Lasercomm demonstration in maritime environment for tactical applications," in *Applications of Lasers for Sensing and Free Space Communications*, OSA Technical Digest Series (Optical Society of America, 2010), paper LSMA2.
6. J. E. Sluz, J. Riggins II, J. C. Juarez, R. M. Sova, D. W. Young, and C. Nelson, "Characterization of data transmission through a maritime free-space optical channel with a custom bit error rate tester," *Proc. SPIE* **7700**, 77000D (2010).
7. C. Nelson, S. Avramov-Zamurovic, R. Malek-Madani, O. Korotkova, R. Sova, and F. Davidson, "Probability density function computations for power-in-bucket and power-in-fiber measurements of an infrared laser beam propagating in the maritime environment," *Proc. SPIE* **8038**, 80380G (2011).
8. L. C. Andrews and R. L. Phillips, *Laser Beam Propagation through Random Media*, 2nd ed. (SPIE, 2005).
9. J. R. W. McLaren, J. C. Thomas, J. L. Mackintosh, K. A. Mudge, K. J. Grant, B. A. Clare, and W. G. Cowley, "Comparison of probability density functions for analyzing irradiance statistics due to atmospheric turbulence," *Appl. Opt.* **51**, 5996–6002 (2012).
10. J. W. Strohbehn, T.-I. Wang, and J. P. Speck, "On the probability density distribution of line-of-sight fluctuations of optical signals," *Radio Sci.* **10**, 59–70 (1975).
11. M. A. Al-Habash, L. C. Andrews, and R. L. Phillips, "Mathematical model for the irradiance probability density function of a laser beam propagating through turbulent media," *Opt. Eng.* **40**, 1554–1562 (2001).
12. L. C. Andrews, R. L. Phillips, and C. Y. Hopen, *Laser Beam Scintillation with Applications* (SPIE, 2001).
13. R. Barakat, "First-order intensity and log-intensity probability density functions of light scattered by the turbulent atmosphere in terms of lower-order moments," *J. Opt. Soc. Am.* **16**, 2269–2274 (1999).
14. O. Steinvali, G. Bolander, M. Petersson, O. Gustafsson, F. Berglund, L. Allard, K. Karlsson, T. Larsson, and F. Gustavsson, "Single- and double-path 10.6 μm laser link measurements over sea water," *Opt. Eng.* **46**, 036001 (2007).
15. R. Mahon, C. I. Moore, H. R. Burris, W. S. Rabinovich, M. Stell, M. R. Suite, and L. M. Thomas, "Analysis of long-term measurements of laser propagation over the Chesapeake Bay," *Appl. Opt.* **48**, 2388–2400 (2009).
16. S. D. Lyke, D. G. Voelz, and M. C. Roggemann, "Probability density of aperture-averaged irradiance fluctuations for long range free space optical communication links," *Appl. Opt.* **48**, 6511–6527 (2009).
17. F. Stromqvist Vetelino, C. Young, L. Andrews, and J. Rekolons, "Aperture averaging effects on the probability density of irradiance fluctuations in moderate-to-strong turbulence," *Appl. Opt.* **46**, 2099–2108 (2007).
18. R. Mahon, C. I. Moore, H. R. Burris, M. Ferraro, W. S. Rabinovich, M. Suite, and L. M. Thomas, "Probability density of irradiance fluctuations observed over terrestrial ranges," *Appl. Opt.* **50**, 6476–6483 (2011).
19. J. Aitchison and J. A. C. Brown, *The Lognormal Distribution* (Cambridge, 1957).
20. O. Korotkova, S. Avramov-Zamurovic, R. Malek-Madani, and C. Nelson, "Probability density function of the intensity of a laser beam propagating in the maritime environment," *Opt. Express* **19**, 20322–20331 (2011).
21. J. H. Churnside and R. J. Hill, "Probability density of irradiance scintillations for strong path-integrated refractive turbulence," *J. Opt. Soc. Am. A* **4**, 727–733 (1987).
22. J. C. Juarez, J. E. Sluz, C. Nelson, M. B. Airola, M. J. Fitch, D. W. Young, D. Terry, F. M. Davidson, J. R. Rottier, and R. M. Sova, "Free-space optical channel characterization in the maritime environment," presented at the SPIE Defense, Security, and Sensing Conference, April, 2010.
23. C. Ruilier and F. Cassaing, "Coupling of large telescopes and single-mode waveguides: application to stellar interferometry," *J. Opt. Soc. Am. A* **18**, 143–149 (2001).